Microstructures of constrained shape memory alloy nanowires under thermal effects

Dhote, R. P., Melnik, R.V.N., Zu, J.W., Wang, L.

Proceedings of the ASME 2010 Conference on Smart Materials, Adaptive Structures and Intelligent Systems (SMASIS-2010), Sept 28 - Oct 1, 2010, Philadelphia, USA, Volume 1, Paper SMASIS2010-3814, pp. 597--603, ISBN 978-0-7918-4415-1, 2010.

Proceedings of the ASME 2010 Conference on Smart Materials, Adaptive Structures and Intelligent Systems
SMASIS2010
September 28 - October 1, 2010, Philadelphia, Pennsylvania, USA

SMASIS2010-3814

MICROSTRUCTURES OF CONSTRAINED SHAPE MEMORY ALLOY NANOWIRES UNDER THERMAL EFFECTS

Rakesh P. Dhote *
Department of Mechanical and Industrial Engineering
University of Toronto
5 King's College Road
Toronto, Canada M5S 3G8
Email: rakesh.dhote@utoronto.ca

Roderick V.N. Melnik
M^2NeT Laboratory
Wilfrid Laurier University
Waterloo, Canada, N2L 3C5
and BCAM, Bizkaia Technology Park
Derio, Spain

Jean W. Zu
Department of Mechanical and Industrial Engineering
University of Toronto
5 King's College Road, Toronto, Canada M5S 3G8

Linxiang Wang
Institute of Mechatronic Engineering
Hangzhou Dianzi University
Hangzhou, China 310 037

ABSTRACT

In this paper, martensitic transformations in constrained Fe-Pd nanowires are studied using a mesoscopic model analyzed in detail numerically in our earlier papers. The dynamics of square-to-rectangular transformation is modeled by using the modified Ginzburg-Landau theory. The simulations are performed accounting for the thermal effects using the coupled equations of non-linear thermoelasticity. Up to date, these effects have typically been neglected in modeling microstructures at the scales of interest considered here. Nanowires of length 2000 nm and widths ranging from 200 nm to 50 nm are simulated to study the effect of size on the microstructure evolution. There exists a critical width below which the size effect is prominent. We present a series of numerical results demonstrating this phenomenon. We also have carried out the study of variations in values of bulk, shear, and Landau constants to understand the difference in evolved microstructure in the coupled and uncoupled physics.

KEYWORDS: Martensite, shape memory effect, square-to-rectangular transformation, Ginzburg-Landau theory, nonlinear thermoelasticity, nanowires, low dimensional nanostructures

INTRODUCTION

Over the last few decades, there has been considerable research interest in Shape Memory Alloys (SMA) due to their current and potential applications resulting from their strongly nonlinear thermo-mechanical properties. SMA's ability to change properties at different temperatures and to recover the original configuration (upon heating) is due to the interesting underlying phenomenon caused by martensitic transformations. The martensitic transformation is a first order diffusionless transformation from a high temperature high symmetry austenite phase to a low temperature low symmetry martensite phase. This transformation gives rise to two unique properties namely, shape memory effect and superelasticity [1]. At larger scales, these properties have been extensively studied in the literature [2].

With the advent in nanotechnology, there is increasing research interest in using SMA at submicron scales. Recent studies reveal interesting properties of SMA at the nanoscale [3, 4], which are not observed at the bulk scale. Sizable surface-to-volume ratios in nanosystems lead to their different mechanical

*Address all correspondence to this author.

behaviors [4–6]. Such nanosystems present an important building block in a range of potential applications such as MEMS and NEMS technologies [7,8], biomechanical and medicine applications [9–11] to name just a few. In these and many other applications our better understanding of nanowire properties at the nanoscale becomes increasingly important.

Recent studies on nanowires [12–14] were carried out to understand their mechanical properties at the nanoscale. In [6], the authors studied the microstructure and mechanical properties of the constrained SMA nanowires and nanograins analyzing the uncoupled physics with a mesoscopic model. Except of a few exceptions (e.g. [15]) up to date, the thermal effects have been neglected so far at the scales of interest considered here.

In this contribution, we present a relatively simple and computationally inexpensive mesoscopic model based on the previous works [16,17] to study the phase transformation and mechanical properties of constrained SMA nanowires using the coupled equations of non-linear thermoelasticity. Square-to-rectangular transformations are used to study the SMA dynamics of FePd nanowires and nanograins.

MATHEMATICAL MODEL FOR SMA DYNAMICS

SMA exhibit first order solid-solid phase transformations like cubic-to-tetragonal (InTl, FePd), cubic-to-orthorhombic (CuAlNi, NiTiCu), cubic-to-monoclinic-I (NiTi, CuZr), tetragonal-to-orthorhombic ($YBa_2Cu_3O_{t-\delta}$) etc. In the general case, there exists 24 possible martensitic variants in three dimensions. The simplified two dimensional representatives like square-to-rectangular, square-to-rhombus have been studied to understand the SMA dynamics. In this work, we use the coarse square-to-rectangular transformation model developed in the previous work [16–19] to simulate the face centered cubic (FCC) to face centered tetragonal (FCT) transformation in FePd alloy.

To model the SMA dynamics, we need the free energy of the system. The free energy consists of homogeneous part i.e. the energy required for the first order phase transformation and the inhomogeneous part for maintaining the different variants in the domain. The free energy is derived on the basis of symmetric strain tensor. We base the free energy function on the Landau theory of phase transformations. This theory is based on the non-convex free energy function of the non-linear continuum thermodynamic model of phase transformations. The local minima of the free energy function with respect to the deformation gradient corresponds to stable and metastable states at a given temperature. We use the modified Ginzburg-Landau free energy function $\mathscr{F}$ used in the earlier works ([16,18,19] and references therein) and [6] as

$$\mathscr{F}(\theta,\varepsilon) = \frac{A_1}{2}\left[e_1 - x_{12}(e_2)^2\right]^2 + \frac{A_3}{2}e_3^2 + \mathscr{F}_l(\theta,\varepsilon) + \mathscr{F}_g(\nabla e_2),$$

$$\mathscr{F}_l(\theta,\varepsilon) = \frac{A_{22}}{2}\frac{\theta-\theta_m}{\theta_m}e_2^2 - \frac{A_{24}}{4}e_2^4 + \frac{A_{26}}{6}e_2^6,$$

$$\mathscr{F}_g(\nabla e_2) = \frac{k_g}{2}\left[\left(\frac{\partial e_2}{\partial x}\right)^2 + \left(\frac{\partial e_2}{\partial y}\right)^2\right], \quad (1)$$

Here e_1, e_2 and e_3 are the hydrostatic, deviatoric and shear strain respectively defined as $e_1 = (\varepsilon_{xx}+\varepsilon_{yy})/\sqrt{2}$, $e_2 = (\varepsilon_{xx}-\varepsilon_{yy})/\sqrt{2}$, $e_3 = (\varepsilon_{xy}+\varepsilon_{yx})/2$, where $\varepsilon_{ij} = [(\partial u_i/\partial x_j)+(\partial u_j/\partial x_i)]/2$ is a Cauchy-Lagrange strain tensor (with the repeated index convention used); u_i, i $= 1,2$ are displacements along x and y directions respectively, θ is the material temperature, θ_m is the austenite-martensite transformation temperature, x_{12} is the volume fraction, A_1 is the bulk constant, A_3 is the shear constant, A_{22}, A_{24}, A_{26} are the Landau constants and k_g is the Ginzburg coefficient.

The first two term in free energy equation Eqn. (1) stabilizes the twin structure for temperature less than θ_m in which the two martensitic variants appear alternatively in $[11]$ and $[\bar{1}1]$ directions [20] as schematically shown in Fig. 1. In addition, the second term also considers the effect of volume fraction x_{12}. The Landau free energy term $\mathscr{F}_l$ defines the first-order phase transformation. It is a convex function of e_2. The deviatoric strain e_2 is used as an order parameter (OP) to characterize the austenite ($e_2 = 0$) and martensite phase ($e_2 \neq 0$) in the microstructure. When the temperature is higher than θ_m, the energy function has only one minima corresponding to the austenite. When the temperature is lower than θ_m, e_2 becomes non-convex and has two local minima corresponding to the two martensite variants. When the temperature is around θ_m, the Landau free energy has three minima, two of which correspond to martensitic phases and the remaining one corresponding to austenite. The Ginzburg term $\mathscr{F}_g$ in Eqn. (1) is proportional to the square of strain gradient. The strain gradient part contributes to inhomogeneous strains. This term does not contribute to the bulk energy and is included to account for the presence of domain walls. It gives non-zero width to austenite-martensite and martensite-martensite interfaces. Since there is no gradient within austenite and martensite, it plays a role similar to interface energy (both austenite-martensite and martensite-martensite). This gradient prevents the system from creating an infinite number of interfaces [17,21].

The dynamics of SMA is highly dependent on the temperature. The SMAs may exhibit ferroelastic, pseudo-elastic and elastic behavior at low, intermediate and high temperatures. This wide range of qualitative behaviors can be captured in the simulations by considering the coupling effects between structural and thermal fields. We base our mathematical model on the three fundamental laws, conservation of mass, linear momentum and energy balance, in the way described previously in [22].
The stresses acting in the system can be calculated by taking derivative of free energy Eqn. (1) with respect to strain com-

ponent as

$$\sigma_{ij}(\mathbf{r},t) = \frac{\delta \mathscr{F}}{\delta \varepsilon_{ij}(\mathbf{r},t)}, \tag{2}$$

$$\begin{aligned}
\sigma_{11} &= \sqrt{2}(Ae_2 - 2Be_2^3 + 3Ce_2^5 + De_1 - 2De_1e_2x_{12} \\
&\quad - De_2^2x_{12} + 2De_2^3x_{12}^2) - k_g\,(u_{1xxx} + u_{1xxy})\,, \\
\sigma_{12} &= E\varepsilon_{xy} + k_g\,(u_{2xxy} + u_{2xyy})\,, \\
\sigma_{21} &= E\varepsilon_{xy} + k_g\,(u_{1xxy} + u_{1xyy})\,, \\
\sigma_{22} &= \sqrt{2}(-Ae_2 + 2Be_2^3 - 3Ce_2^5 + De_1 + 2De_1e_2x_{12} \\
&\quad - De_2^2x_{12} - 2De_2^3x_{12}^2) - k_g\,(u_{2xyy} + u_{2yyy})\,,
\end{aligned} \tag{3}$$

with coefficients $A = (A_{22}(\theta - \theta_m))/(2\theta_m)$, $B = A_{24}/4$, $C = A_{26}/6$, $D = A_1/2$ and $E = A_3/2$.
The structural field dynamics of SMA can be described by the following partial differential equation (PDE):

$$\rho \frac{\partial^2 u_i(\mathbf{r},t)}{\partial t^2} = \sum \frac{\partial \sigma_{ij}(\mathbf{r},t)}{\partial r_j} + \eta \nabla^2 \mathbf{v}_i(\mathbf{r},t), \tag{4}$$

where ρ is the mass density, $\mathbf{v}$ is the time derivative of displacement $\mathbf{u}$, η is the damping coefficient. The choice of η may influence the microstructure and mechanical properties.
The governing equation for the conservation law for internal energy [16] is given by

$$\rho \frac{\partial e}{\partial t} - \sigma^T : \nabla \mathbf{v} + \nabla \cdot \mathbf{q} = g, \tag{5}$$

where $\mathbf{q} = -k\nabla\theta$ is the Fourier heat flux vector, k the heat conductance coefficient of the material and g is thermal loading. The internal energy is connected with the free energy $\mathscr{F}(\theta,\varepsilon)$ by

$$e = \mathscr{F}(\theta,\varepsilon) - \theta \frac{\partial \mathscr{F}(\theta,\varepsilon)}{\partial \theta}, \tag{6}$$

On substituting Eqn. (6) in Eqn. (5), the governing PDE for thermal field can be written as

$$C_v \frac{\partial \theta}{\partial t} = k\left(\frac{\partial^2 \theta}{\partial x^2} + \frac{\partial^2 \theta}{\partial y^2}\right) + a_2 \theta e_2 \frac{\partial e_2}{\partial t} + g. \tag{7}$$

where C_v is specific heat constant.
The SMA dynamics now can be modeled by solving the coupled mechanical and thermal field PDEs simultaneously. The results shown in the following sections have been obtained with the multiphysics finite element software COMSOL [23]. In solving Eqn. (4) and Eqn. (7), we had to overcome a number of challenges due to strong inherent non-linear coupling between mechanical and thermal fields.

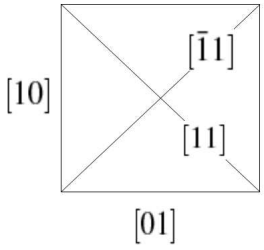

FIGURE 1. Schematic indicating plane directions in the parent crystal

SIMULATIONS OF NANOSYSTEMS

We perform the numerical experiments on nanosystems to study the effect of thermal field on the microstructure and mechanical properties. The numerical experiments are conducted on nanosystems of different sizes. A single crystal austenite (T $> T_m$ (265 K)) is allowed to cool and evolve the microstructure at T = 250 K. The simulations have been carried on nanowires of 2000 nm length and varying widths. The rectangular domain is modeled with sides parallel to [01] and [10] direction of the parent austenite phase. The simulations are performed on FePd nanowires with material parameters found in [6], in particular:
$A_1 = 140$ GPa, $A_3 = 280$ GPa, $A_{22} = 212$ GPa, $A_{24} = 17 \times 10^3$ GPa, $A_{26} = 30 \times 10^6$ GPa, $x_{12} = 0$, T = 250 K , $T_m = 265$ K, $C_v = 350$ Jkg^{-1}K^{-1}, k = 78 Wm^{-1}K^{-1}, $\eta = 0.1$ and $k_g = 1 \times 10^{-4}$.
It is observed that this model is sensitive to damping coefficient η, which affects the microstructure and mechanical properties. The value of damping coefficient is selected to match the mechanical properties of uncoupled physics with [6]. The selected η is used for all the numerical experiments performed in this paper. The boundary conditions for u_i and θ considered for the microstructure evolution are

$$\begin{aligned}
&u_1 = 0, \quad u_2 = 0, \quad \frac{\partial \theta}{\partial n} = 0 \quad \text{on top and bottom edge,} \\
&u_1, u_2 \quad \text{periodic,} \quad \frac{\partial \theta}{\partial n} = 0 \quad \text{on left and right edge,}
\end{aligned} \tag{8}$$

where n is the normal vector to the boundary.

Thermal effect on microstructures in nanowires

The simulations have been performed on nanowires accounting for the coupled structural-thermal physics, to study the microstructure evolution. Following [6, 16], the deviatoric strain e_2 is used as the ordered parameter (OP) to characterize the microstructure phase - austenite ($e_2 = 0$) and martensite ($e_2 \neq 0$). Figure 2 shows the evolved microstructure of the nanowires of different widths considering the coupled structural-thermal physics. Figure 3 shows the evolved microstructure of the nanowires for the same widths for the uncoupled case (con-

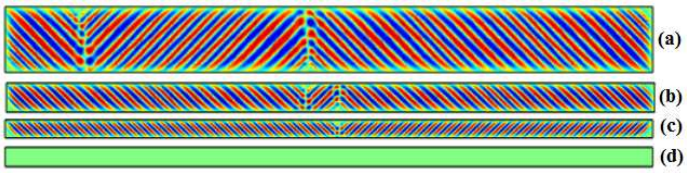

FIGURE 2. (Color online) Evolution of microstructure in nanowires: the coupled structural-thermal physics case for length 2000 nm, x_{12} = 0 and width (a) 200 nm (b) 90 nm (c) 55 nm (d) 52 nm (red and blue indicate martensite variants and green indicates austenite)

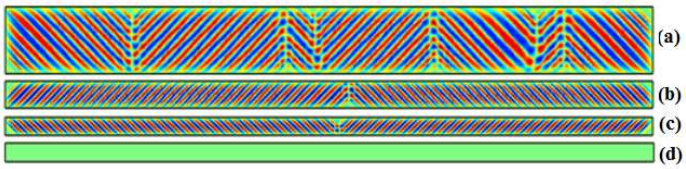

FIGURE 3. (Color online) Evolution of microstructure in nanowires: the uncoupled physics case (considering structural physics only) for length 2000 nm, x_{12} = 0 and width (a) 200 nm (b) 90 nm (c) 55 nm (d) 52 nm (red and blue indicate martensite variants and green indicates austenite)

sidering the structural physics only). The microstructures are different in the coupled and uncoupled physics at higher widths. The twin plane switch direction from $[11]$ to $[11]$ and vice-versa at the twin switching planes for higher widths as schematically shown in Fig. 1. The microstructure difference is not observed at the smaller widths. The martensitic transformation is completely suppressed at smaller widths as the size effect dominates and the austenite remains untransformed. Below a critical width, the confined geometry and/or boundary conditions do not permit the nucleation of martensite. The critical width below which the martensitic transformation ceases in this particular example is around 52 nm. We have also observed that the microstructure and mechanical properties are sensitive to the change of η. The critical width depends on η in Eqn. (4), e.g. when $\eta = 0.01$, the critical width is 92 nm in our earlier presentation [24]. Our current results have been obtained for $\eta = 0.1$. This model qualitatively captures the critical width phenomenon at the nanoscale which is also observed experimentally for NiTi nanowires [25].

Thermal effect on microstructures in square nanoplates

Similar microstructure evolution studies are performed on square nanoplates. Figure 4 shows the evolved microstructures for different sizes of nanosquares for coupled system. The martensitic transformation is completely suppressed below a critical size of 90 nm in this particular example. The higher critical size in square nanoplate as compared to nanowire can be

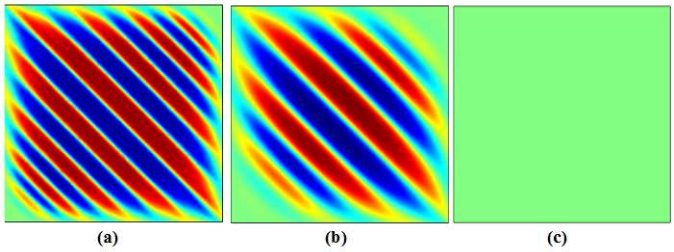

FIGURE 4. (Color online) Evolution of microstructure in square nanoplate with x_{12} = 0 and size (a) 200 nm (b) 95 nm (c) 90 nm (red and blue indicate martensite variants and green indicates austenite)

attributed to its geometric aspect ratio. Due to the symmetric geometry shape, the twin planes are oriented in $[11]$ direction. Because of the confined geometry there is no switching of twin planes as observed in the nonowires.

Coupling physics effect on the mechanical properties

It is important to study the mechanical properties of evolved microstructure in the coupled physics. The tensile test is carried out on the evolved nanowire of length 2000 nm, width 200 nm at constant strain rate. The nanowire is held on one end and displacement equivalent to the strain rate is applied on the opposite end during loading and unloading. Figure 5 shows the stress-strain curves for coupled and uncoupled physics for 5 % strain rate (our earlier results were related to 0.5% strain rate in [24]). The stress-strain curve for uncoupled physics is matched qualitatively with mechanical properties presented in [6]. The properties considered here have not shown a noticeable change in temperature variations in the coupled system. In this particular example, the stress-strain curve has shown a marginal difference in the mechanical properties of coupled and uncoupled physics system, although the difference is observed in the microstructure at higher widths. One reason for this can be explained similar to [6] that the difference in microstructure may or may not lead to change in mechanical properties at the nanoscale. Also it can be that the physical length scale considered here may not show the effect on the mechanical properties in coupled and uncoupled physics, or that there exist no difference in mechanical properties in coupled and uncoupled case for this particular material. These points need further investigations for other materials and transformations.

Effect of variations of A_{22}, A_1 and A_3 on the microstructure

We observe the microstructure differences in the coupled and uncoupled physics for higher widths as shown in Fig. 2 and Fig. 3. To study this further, we carried out the simulations on nanowire of 2000 nm length and 200 nm width to study the ef-

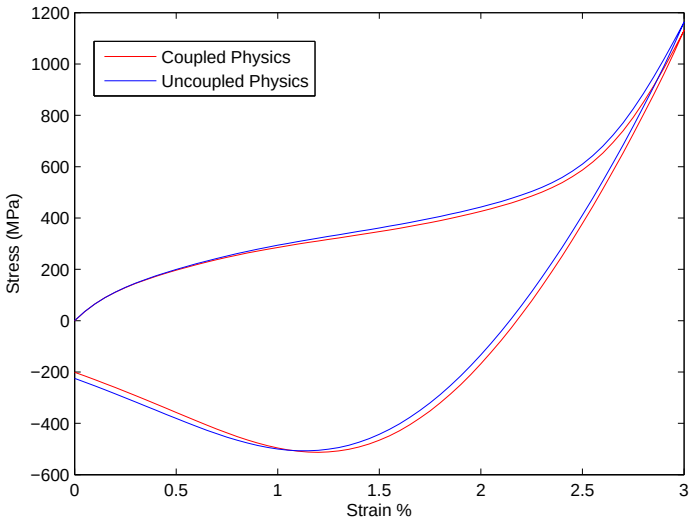

FIGURE 5. (Color online) Mechanical properties of 200 nm wire, x_{12} = 0 and strain rate 5 % for the coupled and uncoupled physics.

fect of variation of bulk constant A_1, shear constant A_3 and Landau constant A_{22} on the evolved microstructure for coupled and uncoupled physics. The effect of variations in these constants have been studied by using the defined parameter - normalized distance of twin switching (or junction) plane $\tilde{x}$ in Eqn. (9) as illustrated in Fig. 6.

$$\tilde{x} = \frac{x_i}{i(l/n)}, \tag{9}$$

where, x_i is the distance of i^{th} switching plane from left edge of geometry, l is the length of the nanowire and n are the total number of switching planes in the nanowire.

Figure (7) shows the effect of variation of A_{22} on the normalized distance of twin switching plane $\tilde{x}$. The A_{22} variation is studied keeping all the other parameters constant during the simulations. In the case of coupled physics, the number of twin switching planes (number of markers) increases with increase in A_{22} upto certain intermediate value and reduces to zero for higher values of A_{22}. For the uncoupled physics, there are no switching of twin planes for lower values of A_{22}. The distribution of twin switching plane is not uniform along the length for both coupled and

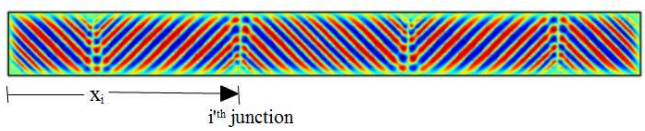

FIGURE 6. (Color online) The quantification parameter $\tilde{x}$ for switching twin plane

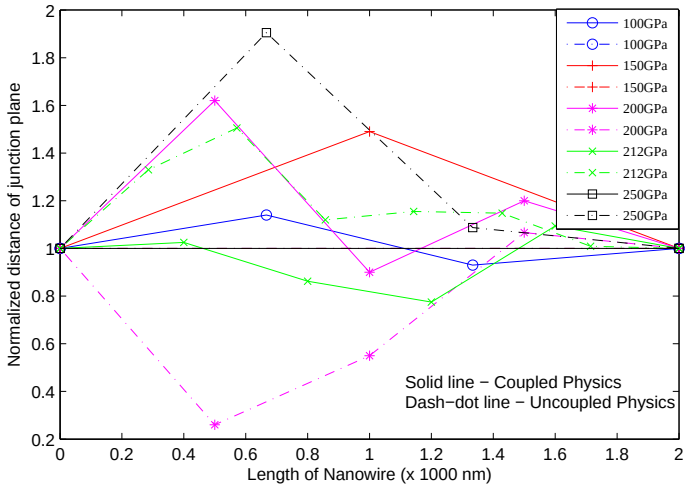

FIGURE 7. (Color online) Effect of A_{22} variation on microstructure evolution in the coupled and uncoupled physics for nanowire of 2000 nm length and 200 nm width. The solid and dash-dot line show the coupled and uncoupled physics data respectively. Markers represent the number of twins, X and Y coordinate represents the ideal location of uniformly distributed twin switching plane along the length and its offset from ideal position respectively.

uncoupled physics. Figure 8 shows the effect of variation of A_1 on the normalized distance of twin switching plane. The values of A_1 are varied over the range keeping all the other parameters constant. The number of twin switching planes remains in certain range for different values of A_1 in the coupled physics. For the uncoupled physics, the number of twin switching planes are high for intermediate values of A_1. The distribution of twin switching plane is not uniform along the length as similarly observed in variation of A_{22}. The number of switching plane decreases with increase in value of A_3 in coupled physics as observed in Fig. 9. There are no twin switching noted for smaller values of A_3 in the uncoupled case. Twin switching occurs for high values of A_3. This study showed that there exist difference between evolved microstructures in the coupled and uncoupled physics with variations in A_{22}, A_1 and A_3. The interaction effect of these parameters can further change the microstructure, which can affect the mechanical properties. This needs to be investigated further.

CONCLUSIONS

We have carried out the analysis on the constrained SMA nanowires accounting for the coupled structural-thermal physics which has not been studied earlier in detail. The results show that the evolved microstructures are different at higher widths for the coupled and uncoupled physics. However, the microstructures are similar for smaller widths for this particular case. There exists a critical width below which martensitic transformation

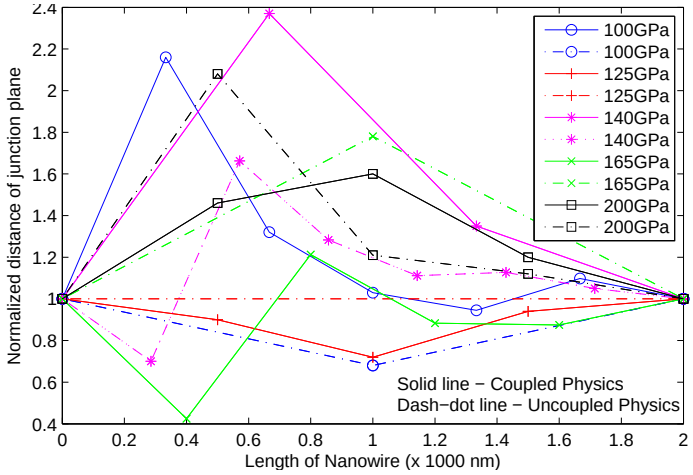

FIGURE 8. (Color online) Effect of A_1 variation on microstructure evolution in the coupled and uncoupled physics for nanowire of 2000 nm length and 200 nm width.

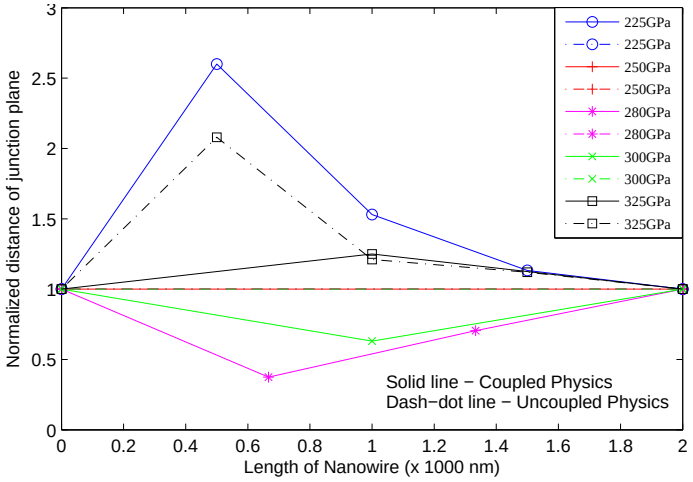

FIGURE 9. (Color online) Effect of A_3 variation on microstructure evolution in the coupled and uncoupled physics for nanowire of 2000 nm length and 200 nm width.

ceases. The critical width arises because of the increase in the surface-to-volume ratio. The critical widths observed in nanowires and square nanoplates in our particular example discussed here are 52 nm and 90 nm, respectively. The higher critical width in square nanoplates can be attributed to their symmetric geometric shapes. The A_{22}, A_1 and A_3 variation studies showed that there is a difference in evolved microstructures in the coupled and uncoupled physics.

ACKNOWLEDGMENT

RD and RM were supported by NSERC and CRC program, Canada. LW was supported by the National Natural Science Foundation of China (Grant No. 10872062).

REFERENCES

[1] Lagoudas, D., 2008. "Shape memory alloys: modeling and engineering applications". Springer, London.

[2] Khandelwal, A., and Buravalla, V., 2009. "Models for shape memory alloy behavior: An overview of modeling approaches". *International Journal of Structural Changes in Solids - Mechanics and Applications*, ***1***(1), pp. 111–148.

[3] Juan, J., No, M., and Schuh, C., 2009. "Nanoscale shape-memory alloys for ultrahigh mechanical damping". *Nature Nanotechnology*, ***4***(7), pp. 415–419.

[4] Liang, W., Srolovitz, D., and Zhou, M., 2007. "A micromechanical continuum model for the tensile behavior of shape memory metal nanowires". *Journal of the Mechanics and Physics of Solids*, ***55***(8), pp. 1729–1761.

[5] Guo, X., Liang, W., and Zhou, M., 2009. "Mechanism for the pseudoelastic behavior of fcc shape memory nanowires". *Experimental Mechanics*, ***49***(2), pp. 183–190.

[6] Bouville, M., and Ahluwalia, R., 2008. "Microstructure and mechanical properties of constrained shape-memory alloy nanograins and nanowires". *Acta Materialia*, ***56***(14), 08, pp. 3558–3567.

[7] Khovaylo, V., A. Kirilin, V. K., G. Lebedev, V. P., Shavrov, V., and Tulaykova, A., 2008. "New composite shape memory functional material for nano and microengineering application". *Proceedings of the 3rd IEEE Int. Conf. on Nano/Micro Engineered and Molecular Systems*, 01, pp. 1231–1236.

[8] Li, M., Tang, H. X., and Roukes, M. L., 2007. "Ultra-sensitive nems-based cantilevers for sensing, scanned probe and very high-frequency applications". *Nature Nanotechnology*, ***2***(2), 02, pp. 114–120.

[9] Barcikowski, S., Hahn, A., Guggenheim, M., Reimers, K., and Ostendorf, A., 2010. "Biocompatibility of nanoactuators: stem cell growth on laser-generated nickeltitanium shape memory alloy nanoparticles". *Journal of Nanoparticle Research*, March.

[10] Yambe, T., Shiraishi, Y., Yoshizawa, M., Tanaka, A., Abe, K., Sato, F., Matsuki, H., Esashi, M., Haga, Y., Maruyama, S., Takagi, T., Luo, Y., Okamoto, E., Kubo, Y., Osaka, M., Nanka, S., Saijo, Y., Mibiki, Y., Yamaguchi, T., Shibata, M., and Nitta, S., 2003. "Artificial myocardium with an artificial baroreflex system using nano technology". *Biomedicine and Pharmacotherapy*, ***57***, pp. 122–125.

[11] Samaroo, H., Lu, J., , and Webster, T., 2003. "Enhanced endothelial cell density on niti surfaces with submicron to nanometer roughness". *International Journal of*

Nanomedicine, ***3***(1), pp. 75–82.

[12] Juan, J. S., No, M. L., and Schuh, C. A., 2008. "Superelasticity and shape memory in micro- and nanometer-scale pillars". *Advanced Materials (FRG)*, ***20***(2), pp. 272–278.

[13] Frick, C. P., Lang, T. W., Spark, K., and Gall, K., 2006. "Stress-induced martensitic transformations and shape memory at nanometer scales". *Acta Materialia*, ***54***(8), pp. 2223 – 2234.

[14] Park, H., and Ji, C., 2006. "On the thermomechanical deformation of silver shape memory nanowires". *Acta Materialia*, ***54***(10), pp. 2645–2654.

[15] Patil, S., and Melnik, R., 2009. "Thermoelectromechanical effects in quantum dots". *Nanotechnology*, ***20***, p. 125402.

[16] Wang, L., and Melnik, R., 2008. "Modifying macroscale variant combinations in a two-dimensional structure using mechanical loadings during thermally induced transformation". *Materials Science and Engineering A, Structural Materials: Properties, Microstructures and Processing*, pp. 190–193.

[17] Wang, L., and Melnik, R., 2008. "Simulation of phase combinations in shape memory alloys patches by hybrid optimization methods". *Applied Numerical Mathematics*, ***58***(4), pp. 511–524.

[18] Melnik, R., and Wang, L., 2009. "Developing mesoscopic models describing phase transformations in finite nanowires and nanoplates". pp. 1–4.

[19] Wang, L., and Melnik, R., 2007. "Thermo-mechanical wave propagation in shape memory alloy rod with phase transformations". *Mechanics of Advanced Materials and Structures*, ***14***(8), pp. 665–676.

[20] Onuki, A., 1999. "Pretransitional effects at structural phase transitions". *Journal of the Physical Society of Japan*, ***68***(1), 01, pp. 5–8.

[21] Bouville, M., and Ahluwalia, R., 2009. "Phase field simulations of coupled phase transformations in ferroelastic-ferroelastic nanocomposites". *Phys. Rev. B*, ***79***(9), p. 094110.

[22] Melnik, R., Roberts, A., and Thomas, K., 2002. "Phase transitions in shape memory alloys with hyperbolic heat conduction and differential-algebraic models". *Computational Mechanics*, ***29***, pp. 16–26.

[23] "Comsol multi-physics modeling and simulation software". Website URL `http://www.comsol.com/`.

[24] Melnik, R., Dhote, R., Zu, J., Tsviliuk, O., and Wang, L. "Numerical analysis of complex systems evolution with phase transformations at different spatial scales". *Proceedings of the Tenth International Conference on Computational Technology, submitted 2010*.

[25] Waitz, T., 2004. "Martensitic phase transformations in nanocrystalline niti studied by tem". *Acta Materialia*, ***52***(1), pp. 137–147.